Atmos. Chem. Phys., 17, 8411–8427, 2017
https://doi.org/10.5194/acp-17-8411-2017

Atmospheric Chemistry and Physics
Open Access
EGU

Understanding the primary emissions and secondary formation of gaseous organic acids in the oil sands region of Alberta, Canada

John Liggio[1], Samar G. Moussa[1], Jeremy Wentzell[1], Andrea Darlington[1], Peter Liu[1], Amy Leithead[1], Katherine Hayden[1], Jason O'Brien[1], Richard L. Mittermeier[1], Ralf Staebler[1], Mengistu Wolde[2], and Shao-Meng Li[1]

[1]Air Quality Research Division, Environment and Climate Change Canada, Toronto, Ontario, M3H 5T4, Canada
[2]National Research Council Canada, Flight Research Laboratory, Ottawa, K1A 0R6, Canada

Correspondence to: John Liggio (john.liggio@canada.ca)

Received: 9 March 2017 – Discussion started: 13 March 2017
Revised: 19 May 2017 – Accepted: 5 June 2017 – Published: 11 July 2017

Abstract. Organic acids are known to be emitted from combustion processes and are key photochemical products of biogenic and anthropogenic precursors. Despite their multiple environmental impacts, such as on acid deposition and human–ecosystem health, little is known regarding their emission magnitudes or detailed chemical formation mechanisms. In the current work, airborne measurements of 18 gas-phase low-molecular-weight organic acids were made in the summer of 2013 over the oil sands region of Alberta, Canada, an area of intense unconventional oil extraction. The data from these measurements were used in conjunction with emission retrieval algorithms to derive the total and speciated primary organic acid emission rates, as well as secondary formation rates downwind of oil sands operations. The results of the analysis indicate that approximately 12 t day^{-1} of low-molecular-weight organic acids, dominated by C_1–C_5 acids, were emitted directly from off-road diesel vehicles within open pit mines. Although there are no specific reporting requirements for primary organic acids, the measured emissions were similar in magnitude to primary oxygenated hydrocarbon emissions, for which there are reporting thresholds, measured previously ($\approx$ 20 t day^{-1}). Conversely, photochemical production of gaseous organic acids significantly exceeded the primary sources, with formation rates of up to $\approx$ 184 t day^{-1} downwind of the oil sands facilities. The formation and evolution of organic acids from a Lagrangian flight were modelled with a box model, incorporating a detailed hydrocarbon reaction mechanism extracted from the Master Chemical Mechanism (v3.3). Despite evidence of significant secondary organic acid formation, the explicit chemical box model largely underestimated their formation in the oil sands plumes, accounting for 39, 46, 26, and 23 % of the measured formic, acetic, acrylic, and propionic acids respectively and with little contributions from biogenic VOC precursors. The model results, together with an examination of the carbon mass balance between the organic acids formed and the primary VOCs emitted from oil sands operations, suggest the existence of significant missing secondary sources and precursor emissions related to oil sands and/or an incomplete mechanistic and quantitative understanding of how they are processed in the atmosphere.

1 Introduction

Organic acids are important atmospheric constituents with various sources, sinks, and roles in gas-phase, particle-phase, and precipitation chemistry. Organic acids, some of which are of sufficiently low volatility to contribute to secondary organic aerosol (SOA), are known photochemical products of volatile organic compound (VOC) oxidation. Numerous studies have identified and/or quantified specific organic acids or organic acid functional groups in particulate matter (PM) (Kawamura and Bikkina, 2016; Zhang et al., 2016; Ho et al., 2015; Li et al., 1997), with organic acids often accounting for a significant fraction of PM mass (Duarte et al., 2015; Yatavelli et al., 2015; Sorooshian et al., 2010). While PM-associated organic acids have a long history of measurements (Li and Winchester, 1992), low-molecular-weight organic acids (LMWOAs; $\approx C_1$–$< C_{10}$), found primarily in the gas phase, have only recently received attention, likely due to difficulties associated with their measurement at trace levels.

The advent of real-time instrumentation with organic acid selectivity (Le Breton et al., 2012; Veres et al., 2008; Yatavelli et al., 2012; Lee et al., 2014) and LMWOA satellite retrievals (Cady-Pereira et al., 2014; Shephard et al., 2015; Stavrakou et al., 2012) has helped to shed light on the importance of LMWOAs in various atmospheric chemistry processes.

From the atmospheric chemical process perspective, LMWOAs can be important contributors to precipitation acidity and ionic balance, particularly in remote areas (Khare et al., 1999; Stavrakou et al., 2012), and are expected to become increasingly important as anthropogenic NO_x and SO_x emissions continue to decrease. They are key participants in the aqueous-phase chemistry of clouds and contribute to SOA formation through various reactions within the aqueous portion of the particle phase (Carlton et al., 2007; Ervens et al., 2004; Lim et al., 2010). Furthermore, since organic acids can be photochemical products, they can also serve as indicators of atmospheric transformation processes. Real-time and improved measurements of LMWOAs present a means of testing the validity of current photochemical reaction mechanisms of VOCs from which the LMWOAs are ultimately derived.

From an environmental health perspective, deposition of LMWOAs may have ecosystem impacts as they have been shown to be toxic to various marine invertebrates (Staples et al., 2000; Sverdrup et al., 2001), phytotoxic (Himanen et al., 2012; Lynch, 1977), and interfere with the uptake and mobilization of heavy metals by microbial communities in soils (Song et al., 2016; Menezes-Blackburn et al., 2016). However, studies on the human toxicity of LMWOAs are sparse and the results are unclear (Rydzynski, 1997; Azuma et al., 2016).

The sources of gaseous organic acids are highly varied. Primary sources of organic acids (LMWOAs in particular) include gasoline and diesel vehicle exhaust emissions (Kawamura et al., 2000; Zervas et al., 2001a, b; Wentzell et al., 2013; Crisp et al., 2014), biofuel combustion, biological activity (i.e. direct vegetation emissions), soil emissions, and biomass burning (Chebbi and Carlier, 1996). However, the largest source of LMWOAs is likely to be their formation from the oxidation of VOCs (Paulot et al., 2011; Veres et al., 2011). The most important oxidation pathway leading to their formation is likely to be the gas-phase ozonolysis of alkenes, in which the further reaction of the resulting stabilized biradicals with water (the dominant pathway under tropospheric conditions) will form organic acids as a primary product (Neeb et al., 1997). Other mechanistic routes include the OH-initiated oxidation of aromatic species (Praplan et al., 2014), the decomposition of peroxyacetyl nitrate (Surratt et al., 2009), and the OH oxidation of vinyl alcohols (Andrews et al., 2012). Some volatile organic acids have also been shown to evolve to the gas phase through heterogeneous aerosol reactions (Molina et al., 2004) and/or aqueous chemical reactions involving glyoxal (Carlton et al., 2007). Despite the known primary and secondary sources of LMWOAs, the chemistry forming LMWOAs from their precursors remains poorly understood. Incorporation of known emissions and associated chemistry into global models has repeatedly indicated missing sources, particularly with respect to formic and acetic acids (Ito et al., 2007; Paulot et al., 2011; Von Kuhlmann et al., 2003). While it has been stated that secondary sources of formic acid and acetic acid from biogenic precursors (isoprene in particular) dominate the global budget of these species, studies have demonstrated that large inconsistencies exist between measurements and model predictions in the Northern Hemisphere (Paulot et al., 2011). Potential inconsistencies have not been examined for other LMWOAs. However, given the limited measurements of other LMWOAs, as well as the complex and likely incomplete mechanistic understanding of their formation, larger discrepancies for other LMWOAs are expected. Large model–measurement inconsistencies in the Northern Hemisphere, after having included biogenic secondary sources, suggest the possibility of secondary formation from anthropogenic VOC precursors, accounting for an increased fraction of the global LMWOA budget. This points to the need for further measurements of LMWOAs formed downwind of anthropogenic emissions.

One such anthropogenic source of LMWOA precursors is the oil and gas sector, which has been expanding significantly in North America over the last several decades and has significant VOC precursor emissions (Gilman et al., 2013). Indeed, the formation of a single LMWOA (formic acid) in an oil and gas region of the United States was studied recently (Yuan et al., 2015) during the winter season. The results of that study demonstrated that formic acid was significantly underpredicted when using the current formic acid photochemical mechanism, even after accounting for potential heterogeneous and aqueous formation. Despite an entirely different VOC profile compared to urban areas, secondary formic acid formation remained high in the region, suggesting that anthropogenic VOC precursors from the oil and gas sector are important contributors to formic acid formation.

The oil sands region of Alberta, Canada, represents another important oil- and gas-producing region in North America with relatively large VOC emissions (Li et al., 2017). It is estimated to contain up to 1.7 trillion barrels of highly viscous oil mixed with sand (Alberta Government, 2009) from which oil is recovered through unconventional surface mining or in situ steam-assisted extraction. Rising oil sands oil production has raised concerns over its environmental impacts, including those associated with the deposition of toxic compounds, and the acidification of nearby ecosystems via the deposition of SO_x and NO_x (Jung et al., 2013; Kelly et al., 2009; Kirk et al., 2014). Recent evidence has also indicated that the downwind transformation of oil sands gaseous precursors (intermediate-volatility organic compounds (IVOCs) in particular) into SOA represents a large PM input into the atmosphere (Liggio et al., 2016). The same photochemical processes that give rise to the ob-

served SOA will also lead to various other gas-phase photochemical products that include organic acids. Given that the oil sands activities are surrounded by forests, the oil sands represent an ideal location to study the primary emission and secondary formation of gaseous organic acids from both industrial and biogenic precursors in the absence of other confounding emissions.

In this work, we describe airborne measurements of gaseous LMWOA both directly emitted from oil sands activities (i.e. primary) and formed via secondary reactions of various oil-sands-emitted and/or biogenic hydrocarbon precursors. Through the use of specifically tailored flight patterns and top-down emissions retrieval algorithms, the total (and speciated) primary emission and secondary production rates of LMWOA from the oil sands are derived, from which the relative importance of primary and secondary organic acids to the total organic acid budget in oil sands plumes is evaluated. Through Lagrangian box modelling of successive oil sands plume intercepts, the relative importance of biogenic and anthropogenic precursors within oil sands plumes is examined, providing a means of evaluating our current understanding of organic acid photochemical formation mechanisms for selected LMWOA.

2 Methods

2.1 Aircraft campaign

Airborne measurements of a variety of air pollutants aboard the National Research Council Canada (NRC) Convair 580 aircraft were performed over the Athabasca oil sands region of northern Alberta from 13 August to 7 September 2013 in support of the Joint Canada-Alberta Implementation Plan on Oil Sands Monitoring (JOSM). Details regarding the overarching study objectives, aircraft campaign implementation, and technical aspects have been described previously (Gordon et al., 2015; Liggio et al., 2016). During this study, 22 flights were conducted over the oil sands for a total of approximately 84 h. To quantify the total primary emissions for each facility, 13 of the flights were conducted by flying in the shape of a four- or five-sided polygon, at multiple altitudes, resulting in 21 separate virtual boxes around seven oil sands facilities. In addition, three flights (F7, F19, F20) were conducted to study the photochemical transformation of pollutants downwind of the oil sands (see the Supplement), including the secondary formation of organic acids.

2.2 Gaseous organic acid measurements

Gaseous organic and inorganic acid measurements were conducted aboard the aircraft with a high-resolution time-of-flight chemical ionization mass spectrometer (HR-ToF-CIMS, Aerodyne Research Inc.). A detailed description of the instrument and principles of operation has been given elsewhere (Bertram et al., 2011; Lee et al., 2014) and in the Supplement. Briefly, the HR-ToF-CIMS used in this study was a differentially pumped time-of-flight mass spectrometer configured to use acetate ion as the reagent ion in the ionization of molecules of interest (Veres et al., 2008; Brophy and Farmer, 2015) via the following reaction:

$$CH_3COO^- + HA \rightarrow CH_3COOH + A^-, \quad (R1)$$

where HA is the acid of interest and A^- is the respective anion. Thus, acids with a gas-phase acidity greater than that of acetic acid (Reaction R1) will be ionized and subsequently sent into the mass spectrometer for detection. There is also evidence that acetate dimers can be involved in the ionization process and/or a number of clustering–declustering and deprotonation reactions of acetate with organic acids (Brophy and Farmer, 2015). At the high field strengths (i.e. strong declustering conditions) utilized during this study (Yuan et al., 2016; Brophy and Farmer, 2015), it is expected that such reactions ultimately also lead to a deprotonated acid ion (A^- in Reaction R1). Calibrations of organic acids were conducted both in the field and post study using a liquid calibration unit (LCU, Ionimed Analytik GmbH), which provided a stable gas stream of analytes by volatilizing aqueous organic acid standards of known composition and concentration prepared from pure compounds (> 99 %, Sigma Aldrich). A list of the quantified organic acids is given in Table 1 and includes 18 acids spanning the C_1–C_{10} range.

The HR-ToF-CIMS data were processed using the Tofware software program (Tofwerk AG, Switzerland), using an approach for mass calibration and high-resolution peak fitting that has been described previously (Brophy and Farmer, 2015; Yuan et al., 2016), resulting in an overall conservative uncertainty of ∼ 40 % in the quantified species (Yuan et al., 2016). The accuracy of the mass (m/z) calibration was approximately 5–7 ppm during the campaign. The reagent acetate ion signal during this campaign was approximately 0.9–2.5 × 10^6 counts per second (cps), and was used to normalize the analyte signals during post processing. The mass resolution of the HR-ToF-CIMS during the study was approximately 3000 to 4000 for ions spanning $m/z = 100$ to greater than $m/z = 200$. The quantified ions were predominantly those whose signal dominated the nominal m/z space, minimally perturbed by neighbouring shoulders and thus less affected by uncertainties associated with HR peak fitting (Yuan et al., 2016). Despite the high-mass-resolution, isomeric species (i.e. the same exact mass) that are also acidic in nature (i.e. ionisable) cannot be resolved from each other. For some organic acid species this is not relevant, as no other acidic compounds with the same exact mass are likely to exist in the atmosphere. Such species include formic acid, propionic acid, acrylic acid and pyruvic acid. For all other species, the signal at the exact mass was calibrated with the available surrogate standards listed in Table 1. While this introduces a degree of uncertainty, calibrated response factors across all species and m/z generally did not vary by more than a factor of 2–3 and it is expected that organic acids with

Table 1. Molecular formulas and associated species names for organic acids detected during aircraft measurements.

Molecular formula	Detected ion : nominal m/z	Species name[a]
HCOOH	$HCOO^-$: 45	Formic acid
CH_3COOH	CH_3COO^- : 61	Acetic acid[b]
$C_3H_4O_2$	$C_3H_3O_2^-$: 71	Acrylic acid
$C_3H_4O_3$	$C_3H_3O_3^-$: 87	Pyruvic acid
$C_3H_6O_2$	$C_3H_5O_2^-$: 73	Propanoic acid
$C_4H_6O_2$	$C_4H_5O_2^-$: 85	Methacrylic acid
$C_4H_6O_3$	$C_4H_5O_3^-$: 87	2-oxo-butanoic acid
$C_4H_8O_2$	$C_4H_7O_2^-$: 101	Butyric acid
$C_5H_6O_3$	$C_5H_5O_3^-$: 117	4-oxo-2-pentenoic acid
$C_5H_8O_2$	$C_5H_7O_2^-$: 113	4-pentenoic acid
$C_5H_8O_3$	$C_5H_7O_3^-$: 99	Levulinic acid
$C_5H_{10}O_2$	$C_5H_9O_2^-$: 115	Pentanoic acid
$C_5H_{10}O_3$	$C_5H_9O_3^-$: 101	2-hydroxy-3-methylbutyric acid
$C_6H_{10}O_2$	$C_6H_9O_2^-$: 113	Cyclopentanoic acid
$C_6H_{12}O_2$	$C_6H_{11}O_2^-$: 115	Hexanoic acid
$C_7H_{10}O_2$	$C_7H_9O_2^-$: 125	1-cyclohexenecarboxylic acid
$C_7H_{12}O_2$	$C_7H_{11}O_2^-$:127	6-heptenoic acid
$C_{10}H_{16}O_3$	$C_{10}H_{15}O_3^-$: 183	Pinonic acid

[a] Species name represents the molecule used for calibration, although not all molecular formulas are for unique species. [b] Measured by PTR-ToF-MS; see methods.

the same exact mass will have response factors that vary considerably less than this.

A proton-transfer time-of-flight mass spectrometer (PTR-ToF-MS, Ionicon AnalytiK) was used to measure acetic acid (which cannot be measured with the HR-ToF-CIMS) in real time during each flight. The PTR-ToF-MS is a soft ionization technique that detects VOCs with a proton affinity greater than that of water. This includes species such as unsaturated hydrocarbons, aromatics, and various oxygenated compounds. Details of the PTR-TOF-MS technique and application have been described previously (Graus et al., 2010; De Gouw and Warneke, 2007; Li et al., 2017). The deployment of the PTR-ToF-MS on the aircraft during this study, its calibration, and data processing have been described elsewhere (Li et al., 2017). Acetic acid via the PTR-ToF-MS was calibrated using a method described previously (De Gouw et al., 2003; Zhao and Zhang, 2004) by calculating a response relative to a known and calibrated reference compound (toluene in this case). The response factor for acetic acid (R_{AA}) is calculated as

$$R_{AA} = \frac{k_{AA} T_{AA} R_{Tol}}{k_{Tol} T_{Tol}}, \quad (1)$$

where k refers to the kinetic rate constant for the reaction of acetic acid or toluene with H_3O^+, T is the experimentally determined ion transmission efficiencies ($C_2H_5O_2^+$, $m/z = 61$ and $C_7H_9^+$, $m/z = 93$), and R_{Tol} is the experimentally derived response factor for toluene (using a standard gas cylinder). The response factor for acetic acid calculated in this manner was within 10 % of that derived using a permeation device during previous studies.

2.3 Other supporting measurements

A detailed description of the meteorological variables, aircraft state parameters and a full list of gas–particle measurements is provided elsewhere (Gordon et al., 2015; Liggio et al., 2016) (http://jointoilsandsmonitoring.ca/default.asp?lang=En&n=A743E65D-1). The current work makes use of a subset of these measurements. These include refractory black carbon (BC) measurements via a single-particle soot photometer (SP2, Droplet Measurement Technologies, Boulder, CO, USA), VOC canister sampling followed by offline analysis and nitrogen oxides (NO and NO_2), and ozone measurements (TECO 42i-TL and 49i respectively, Thermo Fisher Scientific, Waltham, MA, USA). Details with respect to supporting measurements are provided in the Supplement.

2.4 Top-down emission rate retrieval algorithm (TERRA)

A top-down emission rate algorithm (TERRA) designed to estimate pollutant transfer rates through virtual boxes or screens from aircraft measurements was used to derive the primary and secondary emission and production rates from the oil sands flights (Gordon et al., 2015 and Supplement). Briefly, primary emissions are derived utilizing box-like aircraft flight patterns surrounding each of the main surface-mining facilities, pollutant measurements at high time reso-

lution, and wind speed, direction, temperature, and pressure data. Organic acid measurements, at high time resolution, can be used directly in TERRA for estimating their primary emissions; however, they are also secondary products, which may form via chemistry in the short distance and time between the source area and the virtual box wall. Hence, direct use of TERRA for estimating primary organic acid emissions may result in their overestimation. Alternatively, organic acid primary emissions are estimated after normalization to BC in the source area and scaling by the BC emissions via an approach that is described in section "Primary LMWOA Emission Rate Estimates".

Secondary formation rates of organic acids were also derived with an extended version of TERRA using Lagrangian transformation flights (F19, F20). The extended TERRA quantifies the mass transfer rate of pollutants (kilograms per hour) across the virtual screens of transformation flights, in the same manner as for virtual box-type flights, and has been described in detail for SOA (Liggio et al., 2016) and in the Supplement. Briefly, for the transformation flights, TERRA is applied to single screens created by stacking horizontal legs of flight tracks at multiple altitudes and spirals. Concentration data are mapped to the screens and interpolated using a simple kriging function. Pollutant concentrations are also extrapolated below the lowest flight altitude (150 m a.g.l.) based on the assumption of a well-mixed layer below the lowest flight track. It has been demonstrated that this extrapolation is the main source of uncertainty in TERRA, resulting in overall uncertainty in the derived pollutant transfer rates of approximately 20 % (Gordon et al., 2015; Liggio et al., 2016).

2.5 Box modelling

A photochemical box model (AtChem Online, atchem.leeds.ac.uk) coupled with the Master Chemical Mechanism (MCM v3.3, University of Leeds, http://mcm.leeds.ac.uk/MCM/) (Jenkin et al., 2012) was used to simulate the individual organic acid (and total) formation and evolution during transformation Flight 19, as well as ozone and free radical production and other photochemical products. The specific data points within the plume to simulate with the model were selected to be those that were very close to being truly Lagrangian in nature as determined from the wind speed, wind direction, and flying time. The successive plume intercepts modelled here, in which the same air parcel was sampled typically within 1 min of its arrival time based on the wind, are depicted in Fig. S1 in the Supplement. The model consisted of an explicit mechanism for 4578 species in 18 045 reactions. Further details with respect to modifications to the MCM for organic acids are given in the Supplement and in Yuan et al. (2015). Photochemical rate constants were calculated using the Tropospheric Ultraviolet and Visible (TUV) radiation model (https://www2.acom.ucar.edu/modeling/tropospheric-ultraviolet-and-visible-tuv-radiation-model) and were constrained along the flight path. Relative humidity, temperature, and pressure were also constrained with measurement data along the flight path. CO and biogenic VOCs (isoprene, α-pinene, and β-pinene) were constrained via measurements along the entire flight path of the aircraft to account for biogenic emissions between screens. Measured cycloalkanes were lumped into cyclohexane (the only cycloalkane in MCM v3.3), and any other VOCs not present in the MCM were lumped into a VOC with similar reactivity in the MCM. The model was initialized and constrained using the measurements of VOCs (including organic acids), NO_x, CO, O_3, SO_2, and other parameters at the first screen. The model was run for 3 h to correspond with the flight time and with a time step of 1 min. BC measurements were used to derive first-order dilution rate constants and applied to all species to account for ongoing dilution. Species within the plume were diluted at every time step with air outside the plume whenever background measurements of the acids were available; otherwise, clean air was used as background.

3 Results and discussion

3.1 Primary LMWOA emission sources

Primary emissions of various pollutants from specific surface-mining oil sands facilities were estimated by flying virtual boxes around operations followed by subsequent analysis using TERRA (Gordon et al., 2015; Liggio et al., 2016; Li et al., 2017). The specific oil sands facilities that were evaluated are shown in Table S1 in the Supplement with corresponding flight numbers and include Syncrude, Suncor, Canadian Natural Resources Limited (CNRL), Shell, and Imperial Oil. The geographical locations of these operations in relation to the entire oil sands region are provided elsewhere (Li et al., 2017). The results of a typical emission flight (F18, Table S1) are shown in Fig. 1 for a C_5 organic acid, after having applied the simple kriging method to derive a continuous concentration surface. The enhancement in the concentration of this C_5 acid on the downwind box wall (Fig. 1) clearly demonstrates that this species is associated with oil sands activities from this particular facility. Similar enhancements for all other measured organic acids at this facility (and others) and during other flights of Table S1 were also observed. While this organic acid and most others are clearly derived from an oil sands source, generally, surface-mining operations consist of a variety of potential pollutant sources as outlined in Fig. 1, including open pit mines, tailing ponds, and processing plants. These sources are all often in close proximity to each other. However, the chemical nature, location, and extent of individual oil sands plumes within facilities, relative to the prevailing winds, can often be used to determine specific sources. For example, while mines and tailing ponds will lead primarily to surface emissions, pro-

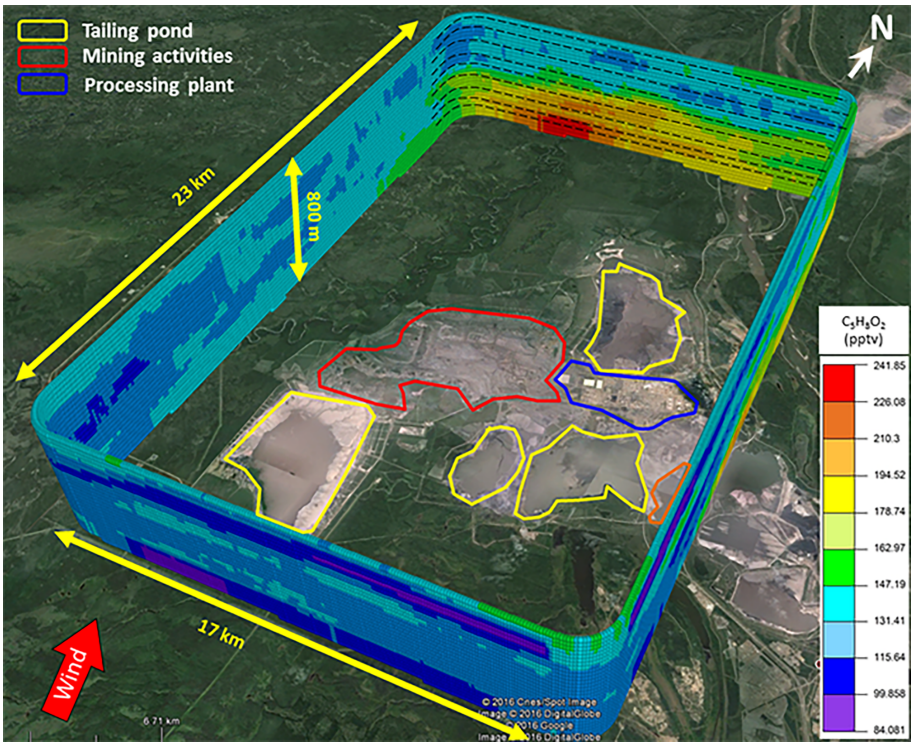

Figure 1. Emissions box flight during Flight 18 on 3 September 2013 (Syncrude – ML) as outputted from TERRA for a typical measured organic acid ($C_5H_8O_2$). Data have been kriged to produce a continuous concentration surface around various oil sands operation sources. Dashed black lines represent approximate locations of the flight tracks on one box wall.

cessing plant emissions may be mostly from elevated stacks, particularly for SO_2 (Gordon et al., 2015). In the case of LMWOA, there is a primary emission source attributed to the use of off-road heavy duty diesel vehicles within the open pit mines, as suggested by several observations described below. Firstly, the prevailing winds and positioning of the concentration enhancements at the box wall of each flight indicate that the open pit mines are the most likely source of the LMWOA emissions (for example in Fig. 1). Within the mines, emissions can arise from the vehicles within the mine, or via volatilization from the mine face itself. Emissions of LMWOA via volatilization is highly unlikely as the oil sands material that is mined is extremely rich in hydrocarbons and deficient in oxygenates and would nonetheless be observed as a more spatially homogenous source (which was not evident). The same is also true for the potential heterogeneous oxidation of the oil sands ore leading to LMWOA. Secondly, LMWOAs during box flights were consistently correlated with BC and not correlated with other species such as SO_2. An example of this relationship is given in Fig. 2a for propionic acid during F18. Figure 2a demonstrates that there is a high degree of similarity between the time series of propionic acid and BC, particularly at the plume intercepts on the virtual box wall. Since the majority of BC emissions within oil sands operations arise from the heavy hauler trucks used in the open pit mining (Wang et al., 2016), the observed LMWOA : BC correlation is consistent with an emission from the large heavy-hauler diesel trucks within the mine and with the known emissions of various LMWOAs from diesel fuel combustion (Kawamura et al., 2000; Wentzell et al., 2013; Crisp et al., 2014; Zervas et al., 2001b). Finally, flights directly over the mines indicate that there are LMWOA emissions at that point specifically (and not elsewhere), and further secondary formation of LMWOA moving away from the primary emission point (see section "Primary LMWOA emission rate estimates"). The relationships and observations above were also evident for other emission flights, and for all other LMWOAs measured. The correlation between LMWOA and BC is subsequently used to derive individual and total LMWOA primary emission rates from various oil sands facilities (after accounting for potential secondary formation), as described further below.

Primary LMWOA emission rate estimates

For conserved and chemically unreactive species, the virtual box flights can be used directly in TERRA to estimate emissions (kilograms per hour) via a mass balance approach. However, the distance between oil sands sources and any given box wall in an emission flight can range from 10 to 15 km. With the average wind speeds during these flights, such a distance corresponds to approximately 10–60 min in

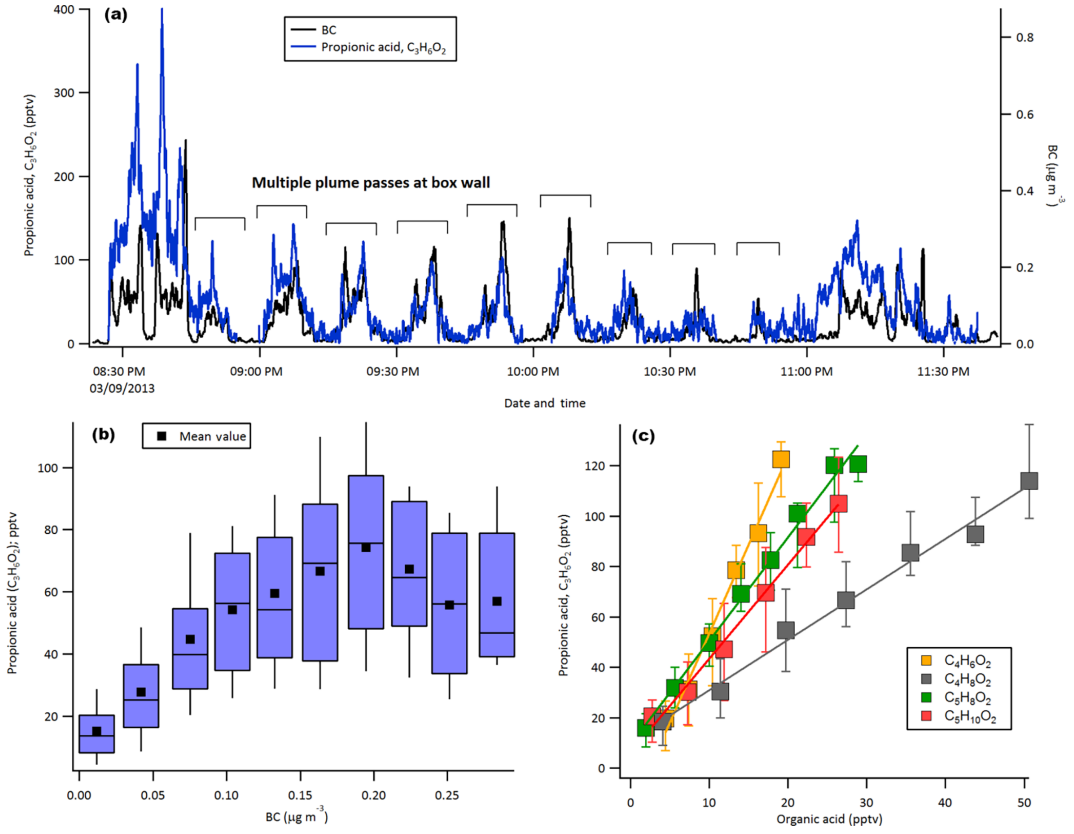

Figure 2. **(a)** Time series of measured propionic acid and BC during Flight 18 (Syncrude – ML). Multiple plume intercepts at the virtual box wall are shown. **(b)** Correlation between propionic acid and BC during F18. Black data points represent the means, and blue boxes and whiskers are the 25th to 75th percentiles and 90th and 10th percentiles respectively. **(c)** Correlations between various measured organic acids during F18. Error bars represent the 25th to 75th percentiles of the data.

transport time. During this time, it is possible that photochemical reactions that could increase or decrease the concentration of a given pollutant at the box wall occur, and hence affect the final emission rate calculated by TERRA. This has been accounted for in the case of VOCs by estimating the rates of oxidation for specific hydrocarbons during travel to the exit of the virtual box, using known rate constants for the reaction of VOC with OH and O_3 (i.e. k_{OH} and K_{O_3}) (Li et al., 2017). This has been shown in most instances to result in small corrections to the TERRA-derived emission rates for the hydrocarbons (Li et al., 2017). The degradation of organic acids during transport to the box wall is expected to be slow since their OH and O_3 rate constants are generally small. However, they are more importantly photochemical products of VOC oxidation. Attempting to correct for the contribution of their photochemical formation prior to input into TERRA is not feasible as it requires detailed knowledge of all oxidation mechanisms leading to LMWOAs and their associated yields. Such information is not available and would nonetheless carry a high degree of uncertainty.

Alternatively, BC is used as a normalizing tracer to estimate facility emission rates. As noted above, the time series of LMWOA and BC are similar (e.g. Fig. 2a), suggesting a common incomplete combustion source from the large mining trucks. The correlation between propionic acid and BC for F18 (for example) is shown in Fig. 2b and indicates that while the two species are correlated, a significant spread in the data exists (denoted by the 25th–75th percentiles), likely caused by a degree of photochemical propionic acid formation while BC is conserved. This is also reflected in the observation that other LMWOAs are more significantly correlated with each other (Fig. 2c) than they are with BC (i.e. LMWOAs are all more similarly formed and lost relative to BC). These observations further imply that the formation of LMWOAs will be reflected in the evolution of the background-subtracted LMWOA to BC ratio (ΔLMWOA / ΔBC) between the emission source and virtual box wall. In this case, the ΔLMWOA / ΔBC at the source (i.e. the emission ratio) can be used to estimate facility primary LMWOA emissions (E_{LMWOA}, kg h^{-1}), when the corresponding BC emissions E_{BC} from the virtual boxes over the individual facilities have been determined using TERRA (Cheng et al., 2017), according to Eq. (2):

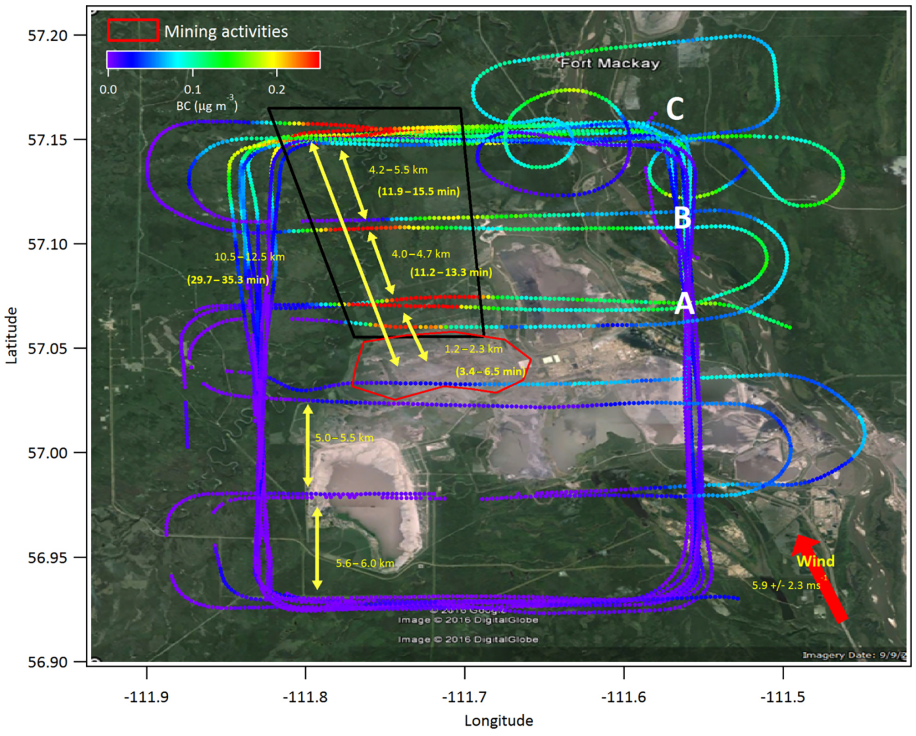

Figure 3. Concentration of BC during emission Flight 18 (Syncrude – ML), showing horizontal transects A–C within the box and closest to the mining emission source (red box). Time in brackets represents the approximate time between horizontal transects or from the approximate centre of the mine to the closest transect. The time is calculated based upon the average wind speed during this portion of the flight. The range in values is based upon differences in time calculated from the northernmost and southernmost legs of transects A–C.

$$E_{\mathrm{LMWOA}} = \left(\frac{\Delta\mathrm{LMWOA}}{\Delta\mathrm{BC}}\right)_{\mathrm{Source}} \times E_{\mathrm{BC}}. \quad (2)$$

LMWOA emission ratios ($(\Delta\mathrm{LMWOA}/\Delta\mathrm{BC})_{\mathrm{source}}$) were derived from flights where horizontal transects between the centre of the open pit mines and the exiting box walls were flown. These flights included F17, F18, and F21 (spanning four facilities) and are depicted in Figs. 3, S2, and S3. These figures indicate the horizontal extent of the BC plumes from the various mines and the approximate times and distances from the approximate centre of a given mine to the various horizontal transects. At the closest transects to the mine centres, the time from emission was estimated to range from approximately 0.3 to 6 min based on the average wind speeds during these flights. This is a time during which photochemical production of the LMWOA is expected to be minimal and the ΔLMWOA / ΔBC ratio should approach the true emission ratio, unlike that expected during the longer transport time from emission to the box wall (10–60 min; see Li et al., 2016) The evolution of ΔLMWOA / ΔBC for the four depicted oil sands operations, at the various horizontal transects of Figs. 3, S2, and S3 (e.g. A, B, C, A_1, B_1, and C_1), are shown in Fig. 4 for a selected organic acid. The boxes in these figures represent the 25th to 75th percentiles of the individual ΔLMWOA / ΔBC ratio values within the plume only, as defined spatially by the BC (which is approximately zero outside of the plume), and at approximately the same altitude. These figures demonstrate a degree of photochemical LMWOA formation when moving from the emission sources to the virtual box walls. Hence, the emission ratios for the various species are considered to be the ratio in the yellow highlighted regions of Fig. 4 (i.e. the closest approach to the mine source – A, A_1, and A_2).

Photochemical formation of organic acids from co-emitted hydrocarbons within the mines is not expected to significantly contribute to the derived emissions ratios in the 0.3 to 6 min travel time. This is particularly likely for the transects closest to the mine sources, as very high co-emitted NO at the source titrates O_3 to levels below 15 ppbv (Fig. S4) and is likely to effectively suppress active photochemistry at the source via OH radicals. Furthermore, most LMWOAs are likely later generation products of VOC oxidation and not likely formed to a great extent in such a short time. Nonetheless, a small secondary LMWOA contribution from co-emitted hydrocarbons to the emission ratios here cannot be entirely ruled out.

The emission ratios (ΔLMWOA / ΔBC) derived for individual LMWOA species for the four facilities shown in Fig. 4 are presented in Fig. S5, in which the error bars represent the 25th to 75th percentiles of the computed ratio data. Gener-

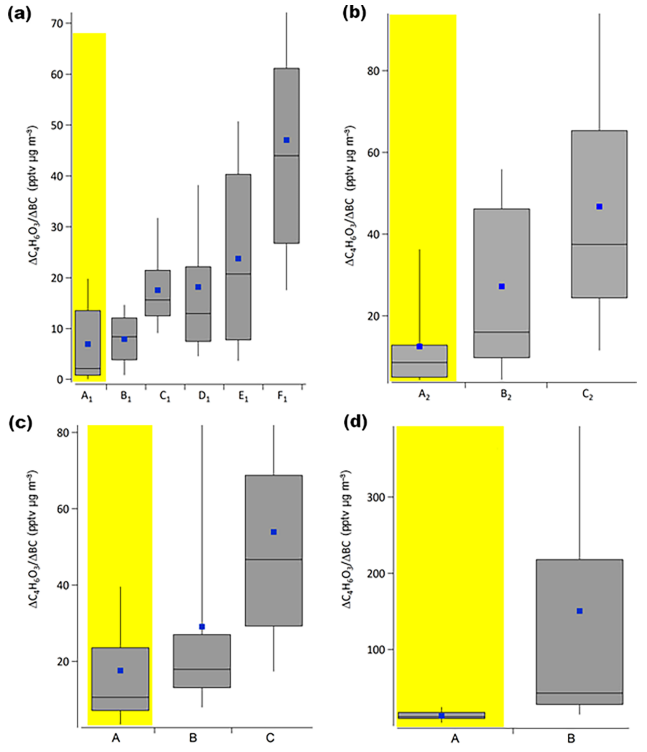

Figure 4. ΔLMWOA / ΔBC evolution (using $C_4H_6O_3$ as an example) across the various transects (A, B, C, etc.) of emission box flights. The yellow highlighted area represents the emission ratio (i.e. closest transect to the open pit mine). Box and whiskers represent the 25th, 75th, 90th, and 10th percentiles. Blue data points represent the mean of the data. **(a)** Derived from F21, Fig. S4 in the Supplement (Syncrude-AU). **(b)** Derived from F21, Fig. S4 (Shell-JP), **(c)** Derived from F18, Fig. 3 (Syncrude-ML). **(d)** Derived from F17, Fig. S3 (CNRL).

ally, the profiles of emission ratios in Fig. S5 are relatively similar to each other, regardless of the facility (means within 15–70 % for individual species). However, the differences between facilities may be attributed to differing emissions control systems between recent and older model mining vehicles. The largest emission ratios are associated with formic and acetic acids, ranging from 412 to 800 pptv/μg m^{-3}, followed by propionic, butyric, and pentanoic acids in the range of 114 to 205 pptv/μg m^{-3}. Other LMWOAs have smaller but non-negligible emission ratios. The corresponding facility LMWOA emission rates (kilograms per hour) derived with Eq. (2) (a primary emission rate estimate) are shown in Fig. S6. Where individual emission ratios for a given facility were not available, the mean of the emission ratios for each species is used to compute the emission rate (i.e. for Suncor – MS and Imperial – KL). Accordingly, the largest primary emission rates are observed for formic and acetic acids (65 and 129 kg h^{-1}, summed across facilities), followed by propionic, butyric, and pentanoic acids at 52, 54, and 40 kg h^{-1} respectively. This corresponds to the fractional contributions to the total measured LMWOA mass emission rate shown in Fig. S7a, in which formic and acetic acids alone account for ∼ 43 % of the primary emissions.

From a facility standpoint, speciated and total measured primary emissions of LMWOA during this study were variable (Fig. S6), with total LMWOA emissions for the Suncor-MS, Syncrude-ML, Syncrude-AU, Shell-MR/JP, CNRL-HOR, and Imperial-KL facilities estimated be 162 ± 22, 108 ± 15, 45 ± 6, 56 ± 8, 60 ± 8, and 19 ± 3 kg h^{-1} respectively. The total primary LMWOA emission rates should also then be somewhat proportional to oil sands oil production, given that LMWOAs are associated with diesel exhaust during mining activities. Since BC emission rates were found to be linearly correlated with the quantity of oil sands mined (Cheng et al., 2017), LMWOA emission rates derived using BC emission rates as the tracer are therefore similarly correlated with the oil sands mined. This correlation suggests that primary LMWOA emissions may also be expected to track increases or decreases in oil sands productivity.

The sum of the measured emission rates for LMWOA (i.e. total primary) is shown in Fig. 5, as well as the measured primary emissions of total and oxygenated VOCs (Li et al., 2017). In total, the oil sands are estimated to emit approximately 12 t day^{-1} of primary LMWOAs (see the Supplement). Relative to the total VOC emitted simultaneously (≈ 214 t day^{-1}), the emission of LMWOA is small, representing an increase to the total VOC emissions of less than 6 %. However, of the total VOC emissions, oxygenated VOCs have been estimated to account for < 10 % (≈ 20 t day^{-1}) (Li et al., 2017) (Fig. 5) and were comprised mainly of methanol, formaldehyde, and acetone. Hence, the LMWOA emissions here represent an increase of up to 60 % to the oxygenated VOC mass emissions, which have previously been unaccounted for and for which there are currently no regulatory reporting requirements.

The primary LMWOA emissions from the oil sands are not easily placed in context, as measurements of emission rates from various other anthropogenic sources are generally not available. On a global scale, primary sources of LMWOAs have been estimated to be very small relative to their photochemical production from a variety of precursor gases (Paulot et al., 2011). This indicates that while possibly important on a regional scale, the primary emitted LMWOAs associated with the oil sands are not expected to contribute significantly to the overall organic acid atmospheric burden both in the Canadian context and/or globally. Given the large emissions of VOCs from oil sands operations (Li et al., 2017), it is likely that secondary formation of LMWOAs from precursors derived from oil sands is more significant than their primary emissions, a subject to be further explored below.

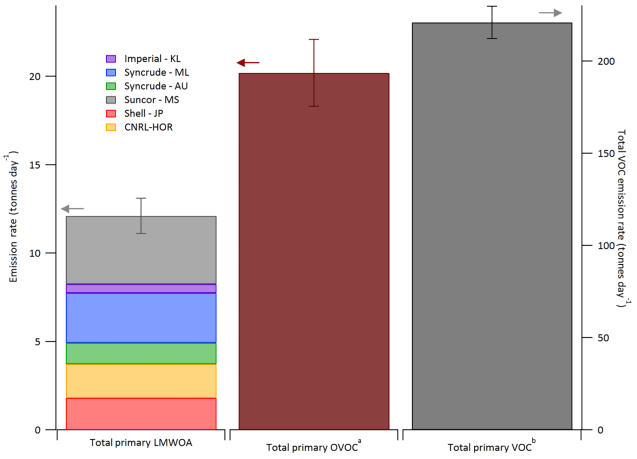

Figure 5. Total daily primary LMWOA emitted in the oil sands (this study, left axis) compared to recently reported total primary VOC (right axis) and total primary oxygenated VOC emissions (left axis). **(a)** As reported in Li et al. (2017). Panel **(b)** includes oxygenates as reported in Li et al. (2017).

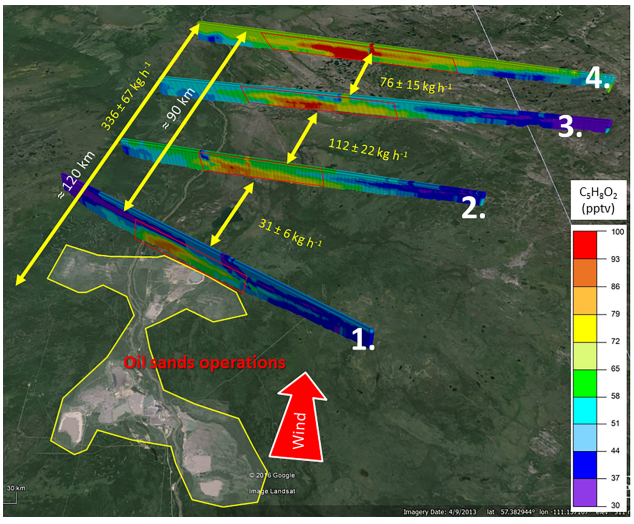

Figure 6. TERRA-derived concentration screens for F19 using $C_5H_8O_2$ as a relevant LMWOA example. The LMWOA transfer rate difference between screens represents the secondary production rate of a given species (yellow text, $219 \pm 43\,\mathrm{kg\,h^{-1}}$ for screens 1–4). The overall rate from the oil sands source region is the integrated LMWOA transfer rate through screen 4 after subtracting a small primary emission rate ($336 \pm 67\,\mathrm{kg\,h^{-1}}$; see text).

3.2 Secondary formation of LMWOA in oil sands plumes

3.2.1 Secondary formation rates

The secondary formation rates of LMWOAs are estimated using a modified version of TERRA with transformation Flights 19 and 20 (see methods, Sect. 2.5). An example of the resultant screens from which secondary formation rates are derived is given in Fig. 6 for $C_5H_8O_2$. Using BC measurements to define the spatial dimensions of the oil sands mine plume (red boxes, Fig. 6), the formation rates for any specific LMWOA is given as the difference in transfer rates between screens (1 to 4). Accordingly, for $C_5H_8O_2$, approximately $219 \pm 43\,\mathrm{kg\,h^{-1}}$ is formed downwind of the oil sands in the 3 h between screens 1 and 4. Similarly, the formation rates for all measured LMWOAs between screens 1 and 4 during F19 are shown in Fig. 7a, along with the sum of the estimated primary LMWOA emissions of Fig. S6 (summed over all facilities). From Fig. 7a it is evident that primary emissions of LMWOAs are negligible compared to those formed via oxidation of precursors; the sum of primary emission rates (across all facilities) is on average 30 times lower than the transfer rates through screen 4 (Fig. 7a). Consequently, the total speciated secondary formation rates (between the source area and screen 4, i.e. ≈ 4 h) are given as the transfer rates at screen 4 (kilograms per hour) after having subtracted the small primary emission contributions; these are shown as the green bars in Fig. 7a. During this 4 hr midday time period, individual secondary production rates of LMWOAs ranged from ≈ 20 to $6700\,\mathrm{kg\,h^{-1}}$, dominated by acetic ($\approx 6700\,\mathrm{kg\,h^{-1}}$) and formic acids ($\approx 3200\,\mathrm{kg\,h^{-1}}$), with all other species in the ≈ 20–$500\,\mathrm{kg\,h^{-1}}$ range. On a percent basis, formic and acetic acids together account for $\sim 70\,\%$ of the total estimated secondary LMWOA production rate downwind of the oil sands, with all other organic acid species generally contributing less than 3 % each to the total (Fig. S7b). This is in contrast to the estimated primary emission rates from the oil sands, in which formic and acetic acids accounted for $\sim 43\,\%$ of the total measured primary LMWOA emission rate, with several other species accounting for up to 12 % (Fig. S7a). Such relative differences between LMWOA secondary production and primary emission rate profiles is expected since photochemical formation of LMWOA is likely to occur at rates and via formation mechanisms that will differ from those of primary combustion sources. Furthermore, formic and acetic acids being the lowest MW acids are likely to have many more precursors than other LMWOAs, implying that their relative proportions to the total LMWOA should increase with increasing photochemical processing.

The hourly formation rates of Fig. 7a are further scaled to 1 photochemical day (i.e. $\mathrm{t\,day^{-1}}$) as previously described in detail (Liggio et al., 2016). While oil sands operations are active 24 h per day, a simple scaling up by multiplying the hourly rates by 24 may add significant uncertainty, as photochemistry does not occur uniformly across these hours. Alternatively, the hourly LMWOA production rate (for each hour) was scaled by the time-integrated OH radical concentration, which was modelled with a box model (Liggio et al., 2016). The daily LMWOA production rate is then the sum of the scaled hourly production rates and is shown in Fig. 7b for Flights 19 and 20. Typically, the scaled

daily secondary production rates were ∼ 54 % of the daily rate derived using a simple 24 h multiplier; 184 ± 37 and 173 ± 34 t day^{-1} for F19 and F20 respectively. This estimation neglects the dry deposition of LMWOA, which may be significant. Accounting for the potential deposition of these species (see the Supplement) increases the estimated total secondary LMWOA formation rates even further to 288 ± 58 and 226 ± 45 t day^{-1}. The total LMWOA secondary production rate (excluding deposition as a lower limit) is also compared to the total measured hydrocarbon VOC emissions from oil sands operations in Fig. 7b. On a total mass basis (tonnes per day) LMWOA production is almost as large as the total VOC primary emissions (∼ 214 t day^{-1}) (Li et al., 2017). At least two oxygen atoms are added during oxidation (to form acids), and hence a carbon mass comparison is more relevant and is also shown in Fig. 7b.

This comparison indicates that up to 50 % of the organic carbon mass emitted is transformed into organic acids (i.e. an effective yield of approximately 50 %) in one photochemical day. Conversely, typical yields for LMWOAs from VOCs in smog chamber experiments are less than 10–15 % and often much lower (Paulot et al., 2009; Neeb et al., 1997; Butkovskaya et al., 2006; Berndt and Böge, 2001; Yuan et al., 2015). This suggests that the total primary VOC emissions have been significantly underestimated and that numerous other hydrocarbon species have not been measured, despite having quantified > 150 individual VOC species. This is consistent with the pool of semivolatile and intermediate-volatility compounds (SVOC / IVOC) expected to be emitted (but not measured), which were responsible for the observed SOA in oil sands plumes (Liggio et al., 2016). The ability of semivolatile and intermediate-volatility hydrocarbons to form LMWOAs is unknown. However, IVOC / total VOC emission ratios for the oil sands have been suggested to be large (Liggio et al., 2016), indicating that yields of LMWOAs from these species can have a significant impact on the total LMWOA production rate. However, from a carbon mass balance perspective, even LMWOA yields of ≈ 10 % from IVOCs would require that the total emitted carbon in the form of IVOCs exceeds the measured VOC carbon emissions (≈ 175 t C day^{-1}, Fig. 7b) by at least a factor of 5 in order to produce the ≈ 75 t C day^{-1} of LMWOA estimated in Fig. 7b. While there is no evidence to the contrary, such a large IVOC contribution to total oil sands emissions may be unlikely. This may suggest that LMWOA yields from IVOCs may be larger than typical VOCs. In this regard, recent evidence has suggested that molecular fragmentation during the oxidation of IVOCs, specifically, can dominate over functionalization (and hence SOA formation) in significantly less time than a photochemical day (Lambe et al., 2012). Molecular fragmentation to smaller species such as LMWOAs in the highly photochemically active plumes encountered here (Liggio et al., 2016) could significantly increase LMWOA yields relative to laboratory yields from experiments, which are typically performed at moderate OH and for less time than a photochemical day (Paulot et al., 2009; Praplan et al., 2014). Biogenic hydrocarbons present along the flight track in F19 and F20 also have the potential to contribute to the observed LMWOA production rate and have not been included in the estimates of total oil sands VOC emissions (Fig. 7b) (Li et al., 2017). However, Lagrangian box modelling of F19 indicates that the biogenic contribution to several LMWOAs is relatively small as described in Sect. 3.2.3.

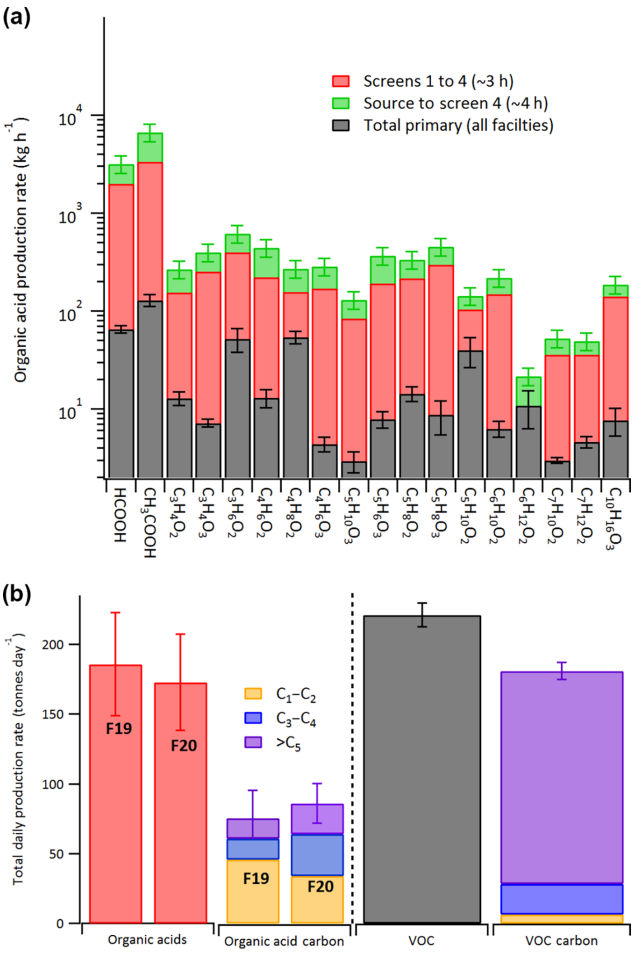

Figure 7. **(a)** Secondary LMWOA production rates (kilograms per hour) derived between screens 1 and 4 of F19 using the TERRA algorithm, and at screen 4 after removing the primary LMWOA contribution (green bars). The primary LMWOA emission rates are also shown (grey bars). **(b)** Total LMWOA secondary production rates (F19 and F20 neglecting deposition) extrapolated to 1 photochemical day compared to total reported primary VOC emissions and carbon associated with these VOC emissions (Li et al., 2017). Data for organic acid and VOC carbon are stacked.

The current LMWOA secondary production rates represent the first such estimates downwind of a large-scale industrial facility. Indeed, measurements of LMWOA secondary production rates from any source are generally not available, and hence placing the LMWOA production from oil sands precursors in context with that of other sources is difficult.

Available estimates of secondary anthropogenic production rates of LMWOAs have been limited to formic and acetic acids, and only in a global context (Ito et al., 2007; Paulot et al., 2011). Nonetheless, the most recent estimates indicate that the sum of secondary anthropogenic and biomass burning sources of formic acid and acetic acid contribute approximately 6.3 and 1.3 Mt per year (Mt yr^{-1}) respectively to the global budget (Paulot et al., 2011). Crudely downscaling (365 days yr^{-1}), this results in a global daily anthropogenic (plus biomass burning) production rate of approximately of 2.1×10^4 t day^{-1} (sum of formic acid and acetic acid). Hence, the combined formic acid and acetic acid secondary production rates observed in oil sands plumes (~ 129 t day^{-1}) likely contribute < 1 % to the global secondary anthropogenic and biomass burning budget. While only qualitative, this comparison suggests that the oil sands are not a major secondary anthropogenic source of formic acid and acetic acid globally.

The impact of the oil sands on a smaller scale (e.g. regional), as a photochemical producer of formic acid and acetic acid (and other organic acids), is not clear since comparative data are not available. However, we note that the total LMWOA formed within a photochemical day of the oil sands in this study (up to ≈ 184 or ≈ 288 t day^{-1} if accounting for deposition) is comparable to the total SO_2 previously reported to be emitted from the oil sands (~ 200–300 t day^{-1}) (Hazewinkel et al., 2008; Jung et al., 2011). The strong acidity associated with sulfur deposition is likely to dominate downwind ecosystem effects. However, the impact of weak acidity on ecosystem acidification has been previously considered (Vet et al., 2014) and may be particularly important in remote areas (Stavrakou et al., 2012; Keene, 1983). The impact of weak acidity downwind of the oil sands specifically is not clear. Critical load exceedances for highly sensitive aquatic systems in northern Alberta have mainly been assessed from the perspective of sulfur and nitrogen (Cathcart et al., 2016; Whitfield et al., 2016). While the impact of the large amount of weak organic acidity formed downwind of the oil sands has not been evaluated, it may have a relevant impact on ecosystem acidification in highly sensitive systems that are approaching their respective sulfur and/or nitrogen critical loads. These results warrant a further investigation of the potential impact of this LMWOA emission and formation in this context.

3.2.2 Modelling secondary LMWOA formation in oil sands plumes

While organic acid secondary production rates are large during F19 and F20 relative to oil sands hydrocarbon primary emissions (Fig. 7), the specific precursor species leading to these observed acids were not clear, including the impact of biogenic volatile organic compound (BVOC) oxidation. However, the Lagrangian nature of F19 allows a comprehensive box model evaluation of the most recent photochemical mechanisms leading to LMWOAs and an estimate of precursor contributions. Flight 19 was modelled for 3 h, beginning at the first screen and ending at the fourth screen, utilizing measurements of all VOCs and inorganic gases at screen 1 as the initial conditions. The most recent Master Chemical Mechanism v3.3, with further improvements for formic acid and acetic acid mechanisms, was used to simulate the secondary chemistry. A detailed description of the box modelling approach is given in methods (Sect. 2.5). As demonstrated in Fig. S8, the box model effectively simulates the evolution of some known organic and inorganic gases, including the oxidative loss of alkenes, alkanes, and aromatics (and others); the cycling of NO_x, and ozone formation; this provides confidence in the interpretation of other aspects of the model output. The comparison between measured and modelled LMWOAs during F19 is shown in Fig. 8. The model output is compared with four specific organic acids (formic, acetic, acrylic, and propionic) as these species are certain to be free of isomeric organic acid interferences in the HR-ToF-CIMS measurements. Figure 8 indicates that the formation of these four species is poorly simulated by the box model. The model and measurement time series diverge quickly (< 30 min), with the model output dominated by dilution (causing the downward trend) while the observed acids increase over 3 h, suggesting that the formation rate of these species is sufficient to overcome the effects of dilution and deposition. After 3 h, the model under-predicts the concentrations of formic, acetic, acrylic, and propionic acids in the plume by factors of 2.6, 2.2, 3.9, and 4.4 respectively. Similarly, the total measured LMWOAs are also under-predicted (Fig. 8) by a factor of 2.9, where 27 modelled organic acids account for 99.8 % of the LMWOA mass as compared to the 18 measured species. Accounting for the depositional losses for these species in the model will increase the model–measurement discrepancy even further. Such poor model–measurement agreement is again consistent with significant unaccounted-for VOC / IVOC emissions, which lead to various LMWOAs, from the oil sands, as was suggested by the unrealistically high effective organic acid yield of 50 % in Fig. 7b (Sect. 3.2.1). This is particularly true for formic acid, whose formation in the MCM has been recently updated (Yuan et al., 2015) and yet remains poorly simulated.

The model output also allows for a more detailed examination of the precursors responsible for a portion of the organic acids observed in oil sands plumes. The relative contribution of various precursor types to the modelled formic, acetic, acrylic, and propionic acids after 3 h during F19 (screen 4) is shown in Fig. 9. These contributions by the precursors indicate that the oxidation of biogenic emissions along the flight track were largely not major contributors to the observed levels of these species relative to the oxidation of oil sands emissions. Formic and acetic acids have received significant attention recently with respect to their photochemical production mechanisms from biogenic species and have been updated in the current MCM used here (see methods). Despite this update, the combined oxidation of isoprene and monoter-

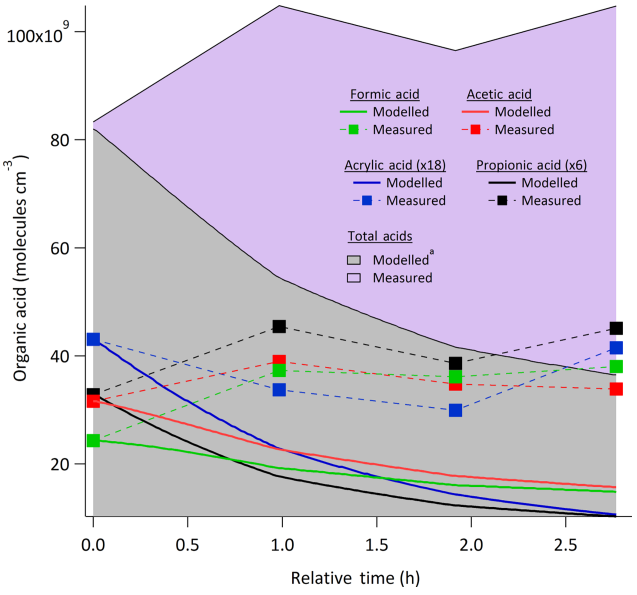

Figure 8. Comparison between specific measured and modelled organic acid species (formic, acetic, acrylic, and propionic) for F19. Total measured and modelled LMWOAs are shown as grey and purple shaded regions. Superscript "a": total modelled LMWOA concentration represents the sum of 27 species, accounting for ∼ 99.8 % of modelled LMWOA mass.

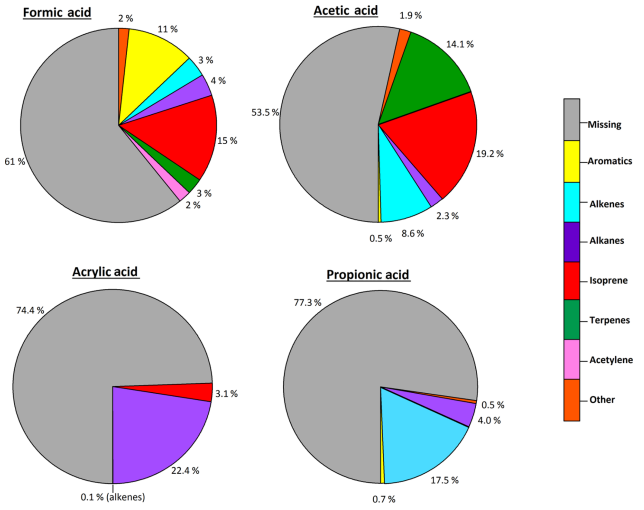

Figure 9. Relative contribution of various precursor hydrocarbon types in the photochemical box model to the modelled secondary production rate after 3 h of evolution during F19, for formic, acetic, acrylic, and propionic acids.

penes accounted for approximately 18 and 33 % of the formic and acetic acid produced after 3 h, with measured aromatics, alkenes, and alkanes accounting for ∼ 2–11 % each. The biogenic contributions to acrylic and propionic acids are even smaller (Fig. 9), with isoprene oxidation contributing ∼ 3 % to acrylic acid formation and propionic acid having no biogenic precursor contribution. The completeness and/or validity of the MCM with respect to acrylic and propionic acids is unclear; it has not been recently updated, as few experimental studies exist to validate MCM yields of these species from various precursors. However, yields from biogenic VOCs for these two species are not likely to exceed those of formic acid and acetic acid, making the contribution to acrylic and propionic acids small.

Undoubtedly, the largest contribution to these four LMWOAs is unaccounted for and labelled as missing in Fig. 9. Such missing precursor sources account for ∼ 54–77 % of production of these species after 3 h of processing. Although other processes such as aqueous and heterogeneous chemistry can lead to LMWOAs and are not included in the MCM mechanism here, their contribution to formic acid formation was estimated to be < 5 % (Yuan et al., 2015). Similarly, fog events and air–snow exchange have no contribution here (i.e. fog and snow were not present). For formic acid, this missing contribution is similar in magnitude to that observed in another oil- and gas-producing region (Yuan et al., 2015). The source of the missing contributions can be a result of several factors: incorrect yields of LMWOA from species currently in the MCM, unknown mechanistic pathways leading to LMWOAs from various MCM precursors, and unmeasured hydrocarbon precursors that hence were not included in the MCM. The first factor appears to be minor, and in the case of formic acid and acetic acid the updated yields from various hydrocarbons in the MCM are considered upper limits (Yuan et al., 2015) and further updates to yield data will likely not result in significantly more formic acid and acetic acid contributions. For the second factor, LMWOA yields from alkanes are not included in the current MCM (with the exception of cyclic alkanes), although limited evidence suggests that some LMWOAs may be indirectly formed via their oxidation (Zhang et al., 2014), but they are insufficient to account for a significant portion of the missing mass in Fig. 9. Given the unrealistically high LMWOA effective yields estimated here (up to 50 %) and the small contribution of BVOC oxidation in these plumes, the third factor is the most likely reason for the missing contributors; their absence may be entirely due to the oxidation of oil-sands-related emissions that were not measured. Furthermore, given the known presence of a large amount of low-volatility oil sands hydrocarbons in these plumes that give rise to SOA (Liggio et al., 2016), it is possible that the large fraction of the missing term will be IVOC, whose photochemical mechanisms have yet to be elucidated, in nature but as noted above are susceptible to significant fragmentation (Lambe et al., 2012), potentially leading to LMWOA.

4 Conclusions

Measurements of 18 gas-phase organic acids have been made in the oil sands region of Alberta, Canada, for the first time,

indicating that they are emitted from primary sources and formed via secondary chemistry in oil sands plumes. The main primary source of these acids is demonstrated to be combustion within open pit mines, leading to primary LMWOA emissions of up to 12 t day^{-1}. This suggests that primary oxygenated emissions from oil sands activities are likely larger than previously considered, with organic acids comprising a large fraction of these emissions.

Despite the potential important contribution of primary LMWOA emissions to the oil sands emissions inventory, secondary formation rates in oil sands plumes were found to be dominant over primary emission rates by more than one order of magnitude; secondary formation rates within 1 photochemical day of the oil sands were in excess of 180 t day^{-1} and were the first estimates of their kind from any industrial or urban–suburban source. Consequently, up to 50 % of the carbon emitted was transformed to organic acids within 1 photochemical day. This is an unusually high effective yield, which suggests the presence unknown–unmeasured hydrocarbons that are capable of producing LMWOAs upon oxidation with significant yields. The Lagrangian nature of several flights during this study also provided a unique opportunity to examine the ability of current photochemical mechanisms to reproduce LMWOA observations. Subsequent box modelling of the evolution of several organic acids over the course of 3 h significantly under-predicts the concentration of simple organic acids. A missing source accounts for the majority of the species measured (54–77 %) but is not related to the oxidation of biogenic species. The poor model predictive ability and the lack of biogenic contribution suggests missing oil sands precursors that are likely to be of intermediate volatility. These results suggest that further work is required to understand the nature of these missing precursors, to elucidate their photochemical pathways leading to LMWOA and other products, and to narrow the model–measurement gap. Finally, the impact of the weak acid deposition to sensitive ecosystems and contribution to overall critical load exceedances is not clear but likely warrants further investigation.

Data availability. Data are available at the Canada-Alberta Oil Sands Environmental Monitoring Information Portal: http://jointoilsandsmonitoring.ca/default.asp?lang=En&n=A743E65D-1, Canada-Alberta Oil Sands, 2016.

The Supplement related to this article is available online at https://doi.org/10.5194/acp-17-8411-2017-supplement.

Competing interests. The authors declare that they have no conflict of interest.

Acknowledgements. We thank the National Research Council (NRC) of Canada flight crew of the Convair 580, the technical support staff of AQRD, and Stewart Cober for the management of the study. The project was supported by the Climate Change and Air Quality Program (CCAP) and the Joint Oil Sands Monitoring program (JOSM).

Edited by: Jennifer G. Murphy
Reviewed by: two anonymous referees

References

Alberta Government: Environmental Management of Alberta's Oil Sands, available at: https://documents.techno-science.ca/documents/EnvironmentAlbertsoilsandsenvironmentalmanagement.pdf (last access: March 2015), 2009.

Andrews, D. U., Heazlewood, B. R., Maccarone, A. T., Conroy, T., Payne, R. J., Jordan, M. J. T., and Kable, S. H.: Photo-tautomerization of acetaldehyde to vinyl alcohol: A potential route to tropospheric acids, Science, 337, 1203–1206, https://doi.org/10.1126/science.1220712, 2012.

Azuma, K., Uchiyama, I., Uchiyama, S., and Kunugita, N.: Assessment of inhalation exposure to indoor air pollutants: Screening for health risks of multiple pollutants in Japanese dwellings, Environ. Res., 145, 39–49, https://doi.org/10.1016/j.envres.2015.11.015, 2016.

Berndt, T. and Böge, O.: Gas-phase reaction of OH radicals with benzene: Products and mechanism, Phys. Chem. Chem. Phys., 3, 4946–4956, https://doi.org/10.1039/b106667f, 2001.

Bertram, T. H., Kimmel, J. R., Crisp, T. A., Ryder, O. S., Yatavelli, R. L. N., Thornton, J. A., Cubison, M. J., Gonin, M., and Worsnop, D. R.: A field-deployable, chemical ionization time-of-flight mass spectrometer, Atmos. Meas. Tech., 4, 1471–1479, https://doi.org/10.5194/amt-4-1471-2011, 2011.

Brophy, P. and Farmer, D. K.: A switchable reagent ion high resolution time-of-flight chemical ionization mass spectrometer for real-time measurement of gas phase oxidized species: characterization from the 2013 southern oxidant and aerosol study, Atmos. Meas. Tech., 8, 2945–2959, https://doi.org/10.5194/amt-8-2945-2015, 2015.

Butkovskaya, N. I., Pouvesle, N., Kukui, A., Mu, Y., and Bras, G. L.: Mechanism of the OH-Initiated oxidation of hydroxyacetone over the temperature range 236–298 K, J. Phys. Chem. A, 110, 6833–6843, https://doi.org/10.1021/jp056345r, 2006.

Cady-Pereira, K. E., Chaliyakunnel, S., Shephard, M. W., Millet, D. B., Luo, M., and Wells, K. C.: HCOOH measurements from space: TES retrieval algorithm and observed global distribution, Atmos. Meas. Tech., 7, 2297–2311, https://doi.org/10.5194/amt-7-2297-2014, 2014.

Canada-Alberta Oil Sands: Air, available at: http://jointoilsandsmonitoring.ca/default.asp?lang=En&n=A743E65D-1, last access: July 2016.

Carlton, A. G., Turpin, B. J., Altieri, K. E., Seitzinger, S., Reff, A., Lim, H. J., and Ervens, B.: Atmospheric oxalic acid and SOA production from glyoxal: Results of aqueous photooxidation experiments, Atmos. Environ., 41, 7588–7602, https://doi.org/10.1016/j.atmosenv.2007.05.035, 2007.

Cathcart, H., Aherne, J., Jeffries, D. S., and Scott, K. A.: Critical loads of acidity for 90,000 lakes in northern Saskatchewan: A novel approach for mapping regional sensitivity to acidic deposition, Atmos. Environ., 146, 290–299, https://doi.org/10.1016/j.atmosenv.2016.08.048, 2016.

Chebbi, A. and Carlier, P.: Carboxylic acids in the troposphere, occurrence, sources, and sinks: A review, Atmos. Environ., 30, 4233–4249, https://doi.org/10.1016/1352-2310(96)00102-1, 1996.

Cheng, Y., Li, S. M., Liu, P., Gordon, M., and Hayden, K.: Black carbon from the Canadian oil sands operations: size distributions and emission rates, in preparation, 2017.

Crisp, T. A., Brady, J. M., Cappa, C. D., Collier, S., Forestieri, S. D., Kleeman, M. J., Kuwayama, T., Lerner, B. M., Williams, E. J., Zhang, Q., and Bertram, T. H.: On the primary emission of formic acid from light duty gasoline vehicles and ocean-going vessels, Atmos. Environ., 98, 426–433, https://doi.org/10.1016/j.atmosenv.2014.08.070, 2014.

De Gouw, J. and Warneke, C.: Measurements of volatile organic compounds in the earth's atmosphere using proton-transfer-reaction mass spectrometry, Mass Spectrom. Rev., 26, 223–257, https://doi.org/10.1002/mas.20119, 2007.

De Gouw, J., Warneke, C., Karl, T., Eerdekens, G., Van der Veen, C., and Fall, R.: Sensitivity and specificity of atmospheric trace gas detection by proton-transfer-reaction mass spectrometry, Int. J. Mass spectrom., 223–224, 365–382, https://doi.org/10.1016/S1387-3806(02)00926-0, 2003.

Duarte, R. M. B. O., Freire, S. M. S. C., and Duarte, A. C.: Investigating the water-soluble organic functionality of urban aerosols using c-state NMR and FTIR spectral data, Atmos. Environ., 116, 245–252, https://doi.org/10.1016/j.atmosenv.2015.06.043, 2015.

Ervens, B., Feingold, G., Frost, G. J., and Kreidenweis, S. M.: A modeling of study of aqueous production of dicarboxylic acids: 1. Chemical pathways and speciated organic mass production, J. Geophys. Res., 109, D15205 15201–15220, https://doi.org/10.1029/2003JD004387, 2004.

Gilman, J. B., Lerner, B. M., Kuster, W. C., and De Gouw, J. A.: Source signature of volatile organic compounds from oil and natural gas operations in northeastern Colorado, Environ. Sci. Technol., 47, 1297–1305, https://doi.org/10.1021/es304119a, 2013.

Gordon, M., Li, S.-M., Staebler, R., Darlington, A., Hayden, K., O'Brien, J., and Wolde, M.: Determining air pollutant emission rates based on mass balance using airborne measurement data over the Alberta oil sands operations, Atmos. Meas. Tech., 8, 3745–3765, https://doi.org/10.5194/amt-8-3745-2015, 2015.

Graus, M., Müller, M., and Hansel, A.: High resolution PTR-TOF: Quantification and Formula Confirmation of VOC in Real Time, J. Am. Soc. Mass Spectrom., 21, 1037–1044, https://doi.org/10.1016/j.jasms.2010.02.006, 2010.

Hazewinkel, R. R. O., Wolfe, A. P., Pla, S., Curtis, C., and Hadley, K.: Have atmospheric emissions from the Athabasca Oil Sands impacted lakes in northeastern Alberta, Canada?, Can. J. Fish. Aquat. Sci., 65, 1554–1567, https://doi.org/10.1139/F08-074, 2008.

Himanen, M., Prochazka, P., Hänninen, K., and Oikari, A.: Phytotoxicity of low-weight carboxylic acids, Chemosphere, 88, 426–431, https://doi.org/10.1016/j.chemosphere.2012.02.058, 2012.

Ho, K. F., Huang, R.-J., Kawamura, K., Tachibana, E., Lee, S. C., Ho, S. S. H., Zhu, T., and Tian, L.: Dicarboxylic acids, ketocarboxylic acids, α-dicarbonyls, fatty acids and benzoic acid in $PM_{2.5}$ aerosol collected during CAREBeijing-2007: an effect of traffic restriction on air quality, Atmos. Chem. Phys., 15, 3111–3123, https://doi.org/10.5194/acp-15-3111-2015, 2015.

Ito, A., Sillman, S., and Penner, J. E.: Effects of additional nonmethane volatile organic compounds organic nitrates, and direct emissions of oxygenates organic species of global tropospheric chemistry, J. Geophys. Res.-Atmos., 112, 1–21, https://doi.org/10.1029/2005JD006556, 2007.

Jenkin, M. E., Wyche, K. P., Evans, C. J., Carr, T., Monks, P. S., Alfarra, M. R., Barley, M. H., McFiggans, G. B., Young, J. C., and Rickard, A. R.: Development and chamber evaluation of the MCM v3.2 degradation scheme for β-caryophyllene, Atmos. Chem. Phys., 12, 5275–5308, https://doi.org/10.5194/acp-12-5275-2012, 2012.

Jung, K., Ok, Y. S., and Chang, S. X.: Sulfate adsorption properties of acid-sensitive soils in the Athabasca oil sands region in Alberta, Canada, Chemosphere, 84, 457–463, https://doi.org/10.1016/j.chemosphere.2011.03.034, 2011.

Jung, K., Chang, S. X., Ok, Y. S., and Arshad, M. A.: Critical loads and H+ budgets of forest soils affected by air pollution from oil sands mining in Alberta, Canada, Atmos. Environ., 69, 56–64, https://doi.org/10.1016/j.atmosenv.2012.12.010, 2013.

Kawamura, K. and Bikkina, S.: A review of dicarboxylic acids and related compounds in atmospheric aerosols: Molecular distributions, sources and transformation, Atmospheric Research, 170, 140–160, https://doi.org/10.1016/j.atmosres.2015.11.018, 2016.

Kawamura, K., Steinberg, S., and Kaplan, I. R.: Homologous series of C1–C10 monocarboxylic acids and C1–C6 carbonyls in Los Angeles air and motor vehicle exhausts, Atmos. Environ., 34, 4175–4191, 2000.

Keene, W. C., Galloway, J. N., and Holden Jr., J. R.: Measurement of weak organic acidity from remote areas of the world, J. Geophys. Res., 88, 5122–5130, 1983.

Kelly, E. N., Short, J. W., Schindler, D. W., Hodson, P. V., Ma, M., Kwan, A. K., and Fortin, B. L.: Oil sands development contributes polycyclic aromatic compounds to the Athabasca River and its tributaries, P. Natl. Acad. Sci. USA, 106, 22346–22351, https://doi.org/10.1073/pnas.0912050106, 2009.

Khare, P., Kumar, N., Kumari, K. M., and Srivastava, S. S.: Atmospheric formic and acetic acids: An overview, Rev. Geophys., 37, 227–248, https://doi.org/10.1029/1998RG900005, 1999.

Kirk, J. L., Muir, D. C. G., Gleason, A., Wang, X., Lawson, G., Frank, R. A., Lehnherr, I., and Wrona, F.: Atmospheric deposition of mercury and methylmercury to landscapes and waterbodies of the athabasca oil sands region, Environ. Sci. Technol., 48, 7374–7383, https://doi.org/10.1021/es500986r, 2014.

Lambe, A. T., Onasch, T. B., Croasdale, D. R., Wright, J. P., Martin, A. T., Franklin, J. P., Massoli, P., Kroll, J. H., Canagaratna, M. R., Brune, W. H., Worsnop, D. R., and Davidovits, P.: Transitions from functionalization to fragmentation reactions of laboratory Secondary Organic Aerosol (SOA) generated from the OH oxidation of alkane precursors, Environ. Sci. Technol., 46, 5430–5437, https://doi.org/10.1021/es300274t, 2012.

Le Breton, M., McGillen, M. R., Muller, J. B. A., Bacak, A., Shallcross, D. E., Xiao, P., Huey, L. G., Tanner, D., Coe, H., and Percival, C. J.: Airborne observations of formic acid using a chemical ionization mass spectrometer, Atmos. Meas. Tech., 5, 3029–3039, https://doi.org/10.5194/amt-5-3029-2012, 2012.

Lee, B. H., Lopez-Hilfiker, F. D., Mohr, C., Kurtén, T., Worsnop, D. R., and Thornton, J. A.: An iodide-adduct high-resolution time-of-flight chemical-ionization mass spectrometer: Application to atmospheric inorganic and organic compounds, Environ. Sci. Technol., 48, 6309–6317, https://doi.org/10.1021/es500362a, 2014.

Li, S.-M. and Winchester, J. W.: Water soluble organic constituents in Arctic aerosols and snow pack, Geophys. Res. Lett., 20, 45–48, 1992.

Li, S. M., Macdonald, A. M., Strapp, J. W., Lee, Y. N., and Zhou, X. L.: Chemical and physical characterizations of atmospheric aerosols over southern California, J. Geophys. Res.-Atmos., 102, 21341–21353, 1997.

Li, S.-M., Leithead, A., Moussa, S. G., Liggio, J., Moran, M. D., Wang, D., Hayden, K., Darlington, A., Gordon, M., Staebler, R., Makar, P. A., Stroud, C. A., McLaren, R., Liu, P. S. K., O'Brien, J., Mittermeier, R. L., Zhang, J., Marson, G., Cober, S. G., Wolde, M., and Wentzell, J. J. B.: Differences between measured and reported volatile organic compound emissions from oil sands facilities in Alberta, Canada (2017) Proceedings of the National Academy of Sciences of the United States of America, 114, E3756–E3765, 2017.

Liggio, J., Li, S. M., Hayden, K., Taha, Y. M., Stroud, C., Darlington, A., Drollette, B. D., Gordon, M., Lee, P., Liu, P., Leithead, A., Moussa, S. G., Wang, D., O'Brien, J., Mittermeier, R. L., Brook, J. R., Lu, G., Staebler, R. M., Han, Y., Tokarek, T. W., Osthoff, H. D., Makar, P. A., Zhang, J., Plata, D. L., and Gentner, D. R.: Oil sands operations as a large source of secondary organic aerosols, Nature, 534, 91–94, https://doi.org/10.1038/nature17646, 2016.

Lim, Y. B., Tan, Y., Perri, M. J., Seitzinger, S. P., and Turpin, B. J.: Aqueous chemistry and its role in secondary organic aerosol (SOA) formation, Atmos. Chem. Phys., 10, 10521–10539, https://doi.org/10.5194/acp-10-10521-2010, 2010.

Lynch, J. M.: Phytotoxicity of acetic acid produced in the anaerobic decomposition of wheat straw, J. Appl. Bacteriol., 42, 81–87, 1977.

Menezes-Blackburn, D., Paredes, C., Zhang, H., Giles, C. D., Darch, T., Stutter, M., George, T. S., Shand, C., Lumsdon, D., Cooper, P., Wendler, R., Brown, L., Blackwell, M., Wearing, C., and Haygarth, P. M.: Organic Acids Regulation of Chemical-Microbial Phosphorus Transformations in Soils, Environ. Sci. Technol., 50, 11521–11531, https://doi.org/10.1021/acs.est.6b03017, 2016.

Molina, M. J., Ivanov, A. V., Trakhtenberg, S., and Molina, L. T.: Atmospheric evolution of organic aerosol, Geophys. Res. Lett., 31, 1–5, https://doi.org/10.1029/2004GL020910, 2004.

Neeb, P., Sauer, F., Horie, O., and Moortgat, G. K.: Formation of hydroxymethyl hydroperoxide and formic acid in alkene ozonolysis in the presence of water vapour, Atmos. Environ., 31, 1417–1423, https://doi.org/10.1016/S1352-2310(96)00322-6, 1997.

Paulot, F., Crounse, J. D., Kjaergaard, H. G., Kroll, J. H., Seinfeld, J. H., and Wennberg, P. O.: Isoprene photooxidation: new insights into the production of acids and organic nitrates, Atmos. Chem. Phys., 9, 1479–1501, https://doi.org/10.5194/acp-9-1479-2009, 2009.

Paulot, F., Wunch, D., Crounse, J. D., Toon, G. C., Millet, D. B., DeCarlo, P. F., Vigouroux, C., Deutscher, N. M., González Abad, G., Notholt, J., Warneke, T., Hannigan, J. W., Warneke, C., de Gouw, J. A., Dunlea, E. J., De Mazière, M., Griffith, D. W. T., Bernath, P., Jimenez, J. L., and Wennberg, P. O.: Importance of secondary sources in the atmospheric budgets of formic and acetic acids, Atmos. Chem. Phys., 11, 1989–2013, https://doi.org/10.5194/acp-11-1989-2011, 2011.

Praplan, A. P., Hegyi-Gaeggeler, K., Barmet, P., Pfaffenberger, L., Dommen, J., and Baltensperger, U.: Online measurements of water-soluble organic acids in the gas and aerosol phase from the photooxidation of 1,3,5-trimethylbenzene, Atmos. Chem. Phys., 14, 8665–8677, https://doi.org/10.5194/acp-14-8665-2014, 2014.

Rydzynski, K.: Environmental health criteria for acrylic acid, in: Environmental Health Criteria, 1–103, 1997.

Shephard, M. W., McLinden, C. A., Cady-Pereira, K. E., Luo, M., Moussa, S. G., Leithead, A., Liggio, J., Staebler, R. M., Akingunola, A., Makar, P., Lehr, P., Zhang, J., Henze, D. K., Millet, D. B., Bash, J. O., Zhu, L., Wells, K. C., Capps, S. L., Chaliyakunnel, S., Gordon, M., Hayden, K., Brook, J. R., Wolde, M., and Li, S.-M.: Tropospheric Emission Spectrometer (TES) satellite observations of ammonia, methanol, formic acid, and carbon monoxide over the Canadian oil sands: validation and model evaluation, Atmos. Meas. Tech., 8, 5189–5211, https://doi.org/10.5194/amt-8-5189-2015, 2015.

Song, Y. W., Wang, H. R., Cao, Y. X., Li, F., Cui, C. H., and Zhou, L. X.: Inhibition of low molecular organic acids on the activity of acidithiobacillus species and its effect on the removal of heavy metals from contaminated soil, Huanjing Kexue/Environmental Science, 37, 1960–1967, https://doi.org/10.13227/j.hjkx.2016.05.046, 2016.

Sorooshian, A., Murphy, S. M., Hersey, S., Bahreini, R., Jonsson, H., Flagan, R. C., and Seinfeld, J. H.: Constraining the contribution of organic acids and AMS m/z 44 to the organic aerosol budget: On the importance of meteorology, aerosol hygroscopicity, and region, Geophys. Res. Lett., 37, 1–5, https://doi.org/10.1029/2010GL044951, 2010.

Staples, C. A., Murphy, S. R., McLaughlin, J. E., Leung, H. W., Cascieri, T. C., and Farr, C. H.: Determination of selected fate and aquatic toxicity characteristics of acrylic acid and a series of acrylic esters, Chemosphere, 40, 29–38, https://doi.org/10.1016/S0045-6535(99)00228-3, 2000.

Stavrakou, T., Müller, J. F., Peeters, J., Razavi, A., Clarisse, L., Clerbaux, C., Coheur, P. F., Hurtmans, D., De Mazière, M., Vigouroux, C., Deutscher, N. M., Griffith, D. W. T., Jones, N., and Paton-Walsh, C.: Satellite evidence for a large source of formic acid from boreal and tropical forests, Nature Geosci., 5, 26–30, https://doi.org/10.1038/ngeo1354, 2012.

Surratt, J. D., Chan, A. W. H., Eddingsaas, N. C., Chan, M., Loza, C. L., Kwan, A. J., Hersey, S. P., Flagan, R. C., Wennberg, P. O., and Seinfeld, J. H.: Reactive intermediates revealed in secondary organic aerosol formation from isoprene, P. Natl. Acad. Sci., 107, 6640–6645, 2009.

Sverdrup, L. E., Källqvist, T., Kelley, A. E., Fürst, C. S., and Hagen, S. B.: Comparative toxicity of acrylic acid to marine and freshwater microalgae and the significance for environmental effects assessments, Chemosphere, 45, 653–658, https://doi.org/10.1016/S0045-6535(01)00044-3, 2001.

Veres, P., Roberts, J. M., Warneke, C., Welsh-Bon, D., Zahniser, M., Herndon, S., Fall, R., and de Gouw, J.: Development of negative-ion proton-transfer chemical-ionization mass spectrom-

etry (NI-PT-CIMS) for the measurement of gas-phase organic acids in the atmosphere, Int. J. Mass Spectrom., 274, 48–55, https://doi.org/10.1016/j.ijms.2008.04.032, 2008.

Veres, P. R., Roberts, J. M., Cochran, A. K., Gilman, J. B., Kuster, W. C., Holloway, J. S., Graus, M., Flynn, J., Lefer, B., Warneke, C., and De Gouw, J.: Evidence of rapid production of organic acids in an urban air mass, Geophys. Res. Lett., 38, 1–5, https://doi.org/10.1029/2011GL048420, 2011.

Vet, R., Artz, R. S., Carou, S., Shaw, M., Ro, C. U., Aas, W., Baker, A., Bowersox, V. C., Dentener, F., Galy-Lacaux, C., Hou, A., Pienaar, J. J., Gillett, R., Forti, M. C., Gromov, S., Hara, H., Khodzher, T., Mahowald, N. M., Nickovic, S., Rao, P. S. P., and Reid, N. W.: A global assessment of precipitation chemistry and deposition of sulfur, nitrogen, sea salt, base cations, organic acids, acidity and pH, and phosphorus, Atmos. Environ., 93, 3–100, https://doi.org/10.1016/j.atmosenv.2013.10.060, 2014.

von Kuhlmann, R., Lawrence, M. G., Crutzen, P. J., and Rasch, P. J.: A model for studies of tropospheric ozone and nonmethane hydrocarbons: Model evaluation of ozone-related species, J. Geophys. Res., 108, ACH6-1–ACH6-26, 2003.

Wang, X., Chow, J. C., Kohl, S. D., Percy, K. E., Legge, A. H., and Watson, J. G.: Real-world emission factors for Caterpillar 797B heavy haulers during mining operations, Particuology, 28, 22–30, https://doi.org/10.1016/j.partic.2015.07.001, 2016.

Wentzell, J. J. B., Liggio, J., Li, S. M., Vlasenko, A., Staebler, R., Lu, G., Poitras, M. J., Chan, T., and Brook, J. R.: Measurements of gas phase acids in diesel exhaust: A relevant source of HNCO?, Environ. Sci. Technol., 47, 7663–7671, https://doi.org/10.1021/es401127j, 2013.

Whitfield, C. J., Mowat, A. C., Scott, K. A., and Watmough, S. A.: A modified approach for estimating the aquatic critical load of acid deposition in northern Saskatchewan, Canada, Atmos. Environ., 146, 300–310, https://doi.org/10.1016/j.atmosenv.2016.05.025, 2016.

Yatavelli, R. L. N., Lopez-Hilfiker, F., Wargo, J. D., Kimmel, J. R., Cubison, M. J., Bertram, T. H., Jimenez, J. L., Gonin, M., Worsnop, D. R., and Thornton, J. A.: A chemical ionization high-resolution time-of-flight mass spectrometer coupled to a micro orifice volatilization impactor (MOVI-HRToF-CIMS) for analysis of gas and particle-phase organic species, Aerosol Sci. Technol., 46, 1313–1327, https://doi.org/10.1080/02786826.2012.712236, 2012.

Yatavelli, R. L. N., Mohr, C., Stark, H., Day, D. A., Thompson, S. L., Lopez-Hilfiker, F. D., Campuzano-Jost, P., Palm, B. B., Vogel, A. L., Hoffmann, T., Heikkinen, L., Äijälä, M., Ng, N. L., Kimmel, J. R., Canagaratna, M. R., Ehn, M., Junninen, H., Cubison, M. J., Petäjä, T., Kulmala, M., Jayne, J. T., Worsnop, D. R., and Jimenez, J. L.: Estimating the contribution of organic acids to northern hemispheric continental organic aerosol, Geophys. Res. Lett., 42, 6084–6090, https://doi.org/10.1002/2015GL064650, 2015.

Yuan, B., Veres, P. R., Warneke, C., Roberts, J. M., Gilman, J. B., Koss, A., Edwards, P. M., Graus, M., Kuster, W. C., Li, S.-M., Wild, R. J., Brown, S. S., Dubé, W. P., Lerner, B. M., Williams, E. J., Johnson, J. E., Quinn, P. K., Bates, T. S., Lefer, B., Hayes, P. L., Jimenez, J. L., Weber, R. J., Zamora, R., Ervens, B., Millet, D. B., Rappenglück, B., and de Gouw, J. A.: Investigation of secondary formation of formic acid: urban environment vs. oil and gas producing region, Atmos. Chem. Phys., 15, 1975–1993, https://doi.org/10.5194/acp-15-1975-2015, 2015.

Yuan, B., Liggio, J., Wentzell, J., Li, S.-M., Stark, H., Roberts, J. M., Gilman, J., Lerner, B., Warneke, C., Li, R., Leithead, A., Osthoff, H. D., Wild, R., Brown, S. S., and de Gouw, J. A.: Secondary formation of nitrated phenols: insights from observations during the Uintah Basin Winter Ozone Study (UBWOS) 2014, Atmos. Chem. Phys., 16, 2139–2153, https://doi.org/10.5194/acp-16-2139-2016, 2016.

Zervas, E., Montagne, X., and Lahaye, J.: C1–C5 organic acid emissions from an SI engine: Influence of fuel and air/fuel equivalence ratio, Environ. Sci. Technol., 35, 2746–2751, https://doi.org/10.1021/es000237v, 2001a.

Zervas, E., Montagne, X., and Lahaye, J.: Emission of specific pollutants from a compression ignition engine. Influence of fuel hydrotreatment and fuel/air equivalence ratio, Atmos. Environ., 35, 1301–1306, https://doi.org/10.1016/S1352-2310(00)00390-3, 2001b.

Zhang, X., Schwantes, R. H., Coggon, M. M., Loza, C. L., Schilling, K. A., Flagan, R. C., and Seinfeld, J. H.: Role of ozone in SOA formation from alkane photooxidation, Atmos. Chem. Phys., 14, 1733–1753, https://doi.org/10.5194/acp-14-1733-2014, 2014.

Zhang, Y. L., Kawamura, K., Cao, F., and Lee, M.: Stable carbon isotopic compositions of low-molecular-weight dicarboxylic acids, oxocarboxylic acids, α-dicarbonyls, and fatty acids: Implications for atmospheric processing of organic aerosols, J. Geophys. Res., 121, 3707–3717, https://doi.org/10.1002/2015JD024081, 2016.

Zhao, J. and Zhang, R.: Proton transfer reaction rate constants between hydronium ion (H 3O+) and volatile organic compounds, Atmos. Environ., 38, 2177–2185, https://doi.org/10.1016/j.atmosenv.2004.01.019, 2004.